Available online at www.sciencedirect.com
ScienceDirect
Journal of Nuclear Materials 367–370 (2007) 621–626
journal of nuclear materials
www.elsevier.com/locate/jnucmat

Irradiation-induced impurity segregation and ductile-to-brittle transition temperature shift in high chromium ferritic/martensitic steels

Z. Lu [a,*], R.G. Faulkner [a], P.E.J. Flewitt [b]

[a] IPTME, Loughborough University, Loughborough, Leicestershire LE11 3TU, UK
[b] BNFL British Nuclear Group, Berkeley Centre, Berkeley, Gloucestershire GL13 9PB, UK

Abstract

A model is presented to predict irradiation-induced impurity segregation and its contribution to the ductile-to-brittle transition temperature (DBTT) shift in high chromium ferritic steels. The hardening contribution (dislocation loops, voids and precipitates) is also considered in this study. The predicted results are compared with the experimental DBTT shifts data for irradiated 9Cr1MoVNb and 12Cr1MoVW steels with different grain sizes.

1. Introduction

High chromium ferritic/martensitic steels are one of potential candidate alloys for further fusion reactor applications because of their good thermal expansion properties and excellent irradiation swelling resistance relative to austenitic steels [1]. However, during low temperature irradiation, the Charpy impact test ductile-to brittle transition temperature (DBTT) will increase due to irradiation hardening and embrittlement, which restricts their application. In fission reactor pressure vessel steels, irradiation-induced impurity segregation (RIS), mainly P, plays an import role in irradiation embrittlement [2]. Neutron irradiation induces high P segregation in VVER (Russian type reactor pressure vessel) steels in which the Cr concentration is 1.5–3.3 wt% and low P segregation in the LWR and C–Mn steels in which the Cr concentration is 0.05–0.1 wt% [3]. The existence of Cr or the other carbide-forming elements results in the decrease of free carbon concentration in the matrix by C atom capture to form carbides. It is well known that there is a site competition effect between P and C atoms. Freely C atoms can suppress the P intergranular segregation. For high Cr ferritic steels, the high Cr concentration, usually 9–12 wt%, may reduce the free C population. Thus, it is reasonable to expect that there is a high impurity grain boundary segregation of elements, such as P, in the high Cr ferritic steels subjected to high neutron fluence irradiation. Experimental results [4–6] verified that irradiation induced intergranular segregation of impurity atoms, like P and Si, occurs in several high Cr

* Corresponding author. Tel.: +44 1509 223168; fax: +44 1509 223949.
E-mail address: zheng.lu@lboro.ac.uk (Z. Lu).

0022-3115/$ - see front matter © 2007 Elsevier B.V. All rights reserved.
doi:10.1016/j.jnucmat.2007.03.039

ferritic steels. However, so far, few investigations of intergranular impurity segregation on the DBTT in high Cr ferritic steels have been carried out.

In this study, irradiation-induced intergranular segregation of impurity atoms and its influence on the DBTT in high Cr ferritic steels is investigated.

2. Model

In this paper, we focus on the effect of the irradiation-induced impurity intergranular segregation, such as P, on the DBTT shift in the high Cr ferritic steels. The radiation-induced defect hardening contribution to the DBTT shift is considered, but any helium contribution is neglected.

2.1. Radiation-induced impurity segregation

A solute drag model has been applied successfully to predict the radiation-induced impurity segregation in 9Cr ferritic steel [4]. The maximum neutron irradiation-induced intergranular maximum impurity segregation in ferritic steels is given by [3],

$$C_{\mathrm{br}}^{\mathrm{S}j} = C_{\mathrm{g}}^{\mathrm{S}j}\frac{E_{\mathrm{b(S}j)}^{\mathrm{ip}}}{E_{\mathrm{f}}^{\mathrm{p}}}\left[\frac{C_{\mathrm{g}}^{\mathrm{S}j}\exp\left(\frac{E_{\mathrm{b(S}j)}^{\mathrm{ip}}}{kT}\right)}{\sum_j C_{\mathrm{g}}^{\mathrm{S}j}\exp\left(\frac{E_{\mathrm{b(S}j)}^{\mathrm{ip}}}{kT}\right)}\right] \times\left[1+\frac{BGF(\eta)}{A_{\mathrm{p}}D_{\mathrm{p}}k_{\mathrm{dp}}^2}\exp\left(\frac{E_{\mathrm{f}}^{\mathrm{p}}}{kT}\right)\right]\quad (j=1,2), \tag{1}$$

where $C_{\mathrm{br}}^{\mathrm{S}j}$ is the maximum concentration of solute j possibly on the grain boundary, $C_{\mathrm{g}}^{\mathrm{S}j}$ is the concentration in the matrix, $E_{\mathrm{b(S}j)}^{\mathrm{ip}}$ is the self-interstitial-impurity binding energy, $E_{\mathrm{f}}^{\mathrm{p}}$ is the point-defect formation energy, B is the proportion of freely migrating defects in the matrix, G is the point-defect generation rate, $F(\eta)$ is the recombination rate, A_{p} is a constant associated with the vibrational entropy of atoms around point-defects, D_{p} is the diffusion coefficient of point-defects in the matrix, k_{dp}^2 is the sink strength for point-defects, which is a function of grain size and dislocation density.

The kinetics of radiation-induced segregation can be expressed by

$$\frac{C_{\mathrm{br}}^{\mathrm{S}j}(t)-C_{\mathrm{g}}^{\mathrm{S}j}}{C_{\mathrm{br}}^{\mathrm{S}j}-C_{\mathrm{g}}^{\mathrm{S}j}} = 1-\exp\left(\frac{4D_{\mathrm{c}}^{\mathrm{ip}}t}{\alpha_n^2 d^2}\right)\mathrm{erfc}\left(\frac{2\sqrt{D_{\mathrm{c}}^{\mathrm{ip}}t}}{\alpha_n d}\right), \tag{2}$$

where $C_{\mathrm{br}}^{\mathrm{S}j}(t)$ is the solute concentration at radiation time t, $D_{\mathrm{c}}^{\mathrm{ip}}$ is the diffusion coefficient of the self-interstitial-impurity complexes, α_{n} is the maximum enrichment ratio, given by $\alpha_{\mathrm{n}} = C_{\mathrm{br}}^{\mathrm{S}j}/C_{\mathrm{g}}^{\mathrm{S}j}$ and d is the thickness of the grain boundary.

Site competition effects between P and C are considered in this model. Carbon atoms can occupy preferentially the lattice sites at a grain boundary (GB). This is because the migration of carbon atoms from the matrix to the GB is easier than for P atoms due to their smaller atomic radius and because the binding energy of carbon atoms with GB is higher than the case for P. Here it is assumed that the solutes i and j first segregate to the grain boundary independently by a solute-self-interstitial complex mechanism to obtain segregation levels C_{br}^{si} and $C_{\mathrm{br}}^{\mathrm{S}j}$, then re-distribute there in proportion to their binding energies with the grain boundary. The effect is expressed by

$$C_{\mathrm{br}}^{\mathrm{S}j}(t)^* = C_{\mathrm{br}}^{\mathrm{S}j}(t)\left[\frac{C_{\mathrm{g}}^{\mathrm{S}j}\exp\left(\frac{Q_{\mathrm{S}j}}{kT}\right)}{C_{\mathrm{g}}^{\mathrm{S}i}\exp\left(\frac{Q_{\mathrm{S}i}}{kT}\right)+C_{\mathrm{g}}^{\mathrm{S}j}\exp\left(\frac{Q_{\mathrm{S}j}}{kT}\right)}\right], \tag{3}$$

where $C_{\mathrm{br}}^{\mathrm{S}j}(t)^*$ is the final level of irradiation-induced grain boundary segregation for solute j, $Q_{\mathrm{S}i}$ and $Q_{\mathrm{S}j}$ are the binding energies of the grain boundary with solutes i and j, respectively, and $C_{\mathrm{g}}^{\mathrm{S}i}$ and $C_{\mathrm{g}}^{\mathrm{S}j}$ are matrix concentration of solutes i and j, respectively.

2.2. Irradiation-induced fracture stress shift

The change in irradiation-induced fracture stress is given by [7,8]

$$\Delta\sigma_{\mathrm{F}} = \sqrt{\frac{E\Delta G_k}{\pi d}}, \tag{4}$$

where G_k is the work of fracture allowing for the stress concentration ahead of the crack, d is the grain size, and E is the Young's modulus. The stress concentration effect has been approximated by several workers and a reasonable factor is 100 [16]. Therefore, $\Delta G_k = 100(\gamma_{\mathrm{P}}-\gamma_1)$, where γ_{P} is the energy required to create new surface and to cause dislocation activity ahead of the crack, and γ_1 is the original energy to create unit area of grain boundary. McMahon and Vitek [9] developed a method to relate this quantity to the initial surface energy and the work hardening away from the associated dislocations: $\gamma_{\mathrm{P}} = \gamma_1\exp\{(n+1)\ln(\gamma/\gamma_1)\}$, $n = \frac{\ln\dot{\varepsilon}_{\mathrm{P}}}{\ln\sigma}$, $\dot{\varepsilon}_{\mathrm{p}}$ is plastic strain rate, σ is stress. $\gamma_1 = 2\gamma_{\mathrm{S}}-\gamma_{\mathrm{GB}}$, γ_{S} is the surface energy and γ_{GB} is the grain bound-

ary energy. γ is the new energy required to create a unit area of grain boundary when a segregant is present.

The change in grain boundary energy as a function of the concentration of segregated impurity and the atomic structure of that boundary has been expressed by [8]

$$\gamma - \gamma_1 = -\left(1 - \frac{1}{\Sigma}\right)\frac{d_{GB}}{\Omega} RT \ln[1 - (C - C_0) + b(C - C_0)], \tag{5}$$

where Σ is the coincidence site relationship of the boundary (assumed to be 99 for a random boundary in this work), d_{GB} is the grain boundary thickness, Ω is the molar volume of the matrix, R is the gas constant, T is absolute temperature, C is the irradiation-induced impurity concentration at the grain boundary which is calculated by the Solute Drag model described in Section 2.1, C_0 is the critical impurity concentration for intergranular fracture ($C_0 = 0$ is applied in this study) and b is an enrichment factor given by $b \cong \exp\left(\frac{0.75E_F}{kT}\right)$, where E_F is the formation energy of the impurity atom in the matrix. The parameters used in this model are listed in Table 1.

2.3. Irradiation-induced yield stress shift

The irradiation-induced yield stress increase, $\Delta\sigma_y$, due to the microstructural obstacles (dislocation loops, voids and precipitates), produced during irradiation, can be estimated from dispersive hardening theory [10]:

$$\Delta\sigma_y^2 = \Delta\sigma_{loop}^2 + \Delta\sigma_{void}^2 + \Delta\sigma_{precipitate}^2, \tag{6}$$

where $\Delta\sigma_{loop} = 2\alpha\mu b(N_1 d_1)^{1/2}$, $\Delta\sigma_{void} = 2\alpha\mu b(N_2 d_2)^{1/2}$ and $\Delta\sigma_{precipitate} = \mu b(N_3 d_3)^{1/2}$. α is the barrier strength of loops or voids, μ is the shear modulus of the matrix, b is the Burger's vector, N_i and d_i are the densities and mean sizes of loops, voids and precipitates, respectively.

Table 1
The parameters used in the models

Surface energy, σ_S, Jm^{-2}	1.9
GB fracture energy, σ_1, Jm^{-2}	2.8
GB free energy, σ_{GB}, Jm^{-2}	1.0
Impurity formation energy, E_F, eV	0.14
Work hardening exponent, n	7.5
Atomic volume, Ω, m^3 mol^{-1}	10^{-5}
Grain boundary width, nm	1
Young's modulus, E, GPa	210
Shear modulus, G, GPa	81
Impurity atom radius, a_1, nm	0.109
Matrix atom radius, a_{m1}, nm	0.124
P concentration in matrix , wt%	0.012 (9Cr1MoVNb) [12] 0.016 (12Cr1MoVW) [12]

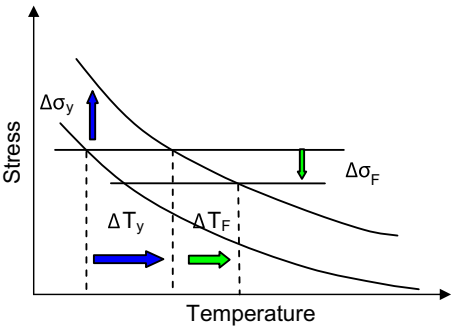

Fig. 1. Schematic relationship of yield stress, fracture stress and DBTT shift ($\Delta\sigma_y$: change in yield stress, $\Delta\sigma_F$: change in facture stress; ΔT_y, ΔT_F: corresponding DBTT shifts).

2.4. Irradiation-induced DBTT shift

The irradiation-induced DBTT shift can be written by [2]

$$\Delta\text{DBTT} = \Delta T_y + \Delta T_F, \tag{7}$$

where ΔT_y is a hardening contribution, and ΔT_F is a non-hardening contribution. The hardening contribution comes from irradiation-induced dislocation loops, voids and precipitates, leading to the increase of yield stress, $\Delta\sigma_y$, and the corresponding decrease of corresponding transition temperature T_y. The non-hardening is due to irradiation-induced intergranular segregation at interfaces, such as grain boundaries, resulting in the decrease of fracture stress $\Delta\sigma_F$ and a shift of ΔT_F, shown schematically in Fig. 1. The correlation of ΔT_y, ΔT_F and $\Delta\sigma_y$, $\Delta\sigma_F$ can be expressed by

$$\begin{aligned} \Delta T_y &= k_1 \Delta\sigma_y, \\ \Delta T_F &= k_2 \Delta\sigma_F, \end{aligned} \tag{8}$$

where k_1 and k_2 are the slopes of yield stress and ultimate stress curves and are evaluated from the experimental data reported in [1] (0.62 and 0.2 are used in this study). This analysis assumes that $\Delta\sigma_y$ is constant with the whole range of temperature. This is not true, $\Delta\sigma_y$ increases with decreasing temperature. This is neglected in this analysis.

3. Results and discussion

There are two segregation peaks in the expected temperature dependence for phosphorus and other

elemental inter-granular segregation. The lower temperature peak is due to irradiation-induced segregation, the higher temperature peak is due to thermal equilibrium segregation. The precise peak position is determined by the material composition and microstructure, the segregating elements, and the irradiation conditions. With the increase of neutron fluence and grain size, irradiation-induced segregation increases. With the increase of dislocation density and free carbon concentration, the impurity segregation decreases. The higher dose rate makes the segregation peak shift to the higher temperature region. A detailed discussion of these effects can be found in [3].

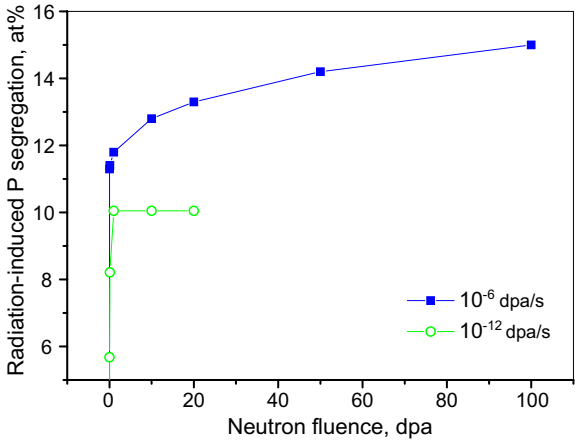

Fig. 2. The calculated P intergranular segregation induced by neutron irradiation under the flux of 10^{-6} and 10^{-12} dpa/s (dislocation density: 10^{15} lines/m^3, grain size: 16 μm, free C: 10 appm).

In a fusion reactor, the structural materials used as a first wall will be subjected to a higher neutron fluence and flux than the RPV steels in a fission reactor. Irradiation-induced P segregation at a fluence of 100 dpa and a flux of 10^{-6} dpa/s at 365 °C is calculated and shown in Fig. 2. Compared to the irradiation at a lower flux typical of a fission reactor (10^{-12} dpa/s), the high flux leads to overall higher impurity segregation at grain boundaries. Radiation-induced segregation of P approaches the saturation at about 1 dpa under a flux of 10^{-12} dpa/s and does not approach saturation at those up to 100 dpa under a flux of 10^{-6} dpa/s. With the increase of neutron fluence, radiation-induced P segregation increases and GB fracture strength decreases according to the analysis given in Section 2.2.

The calculated DBTT shifts are compared with the experimental data for 9Cr1MoVNb and 12Cr1MoVW steels ([11] and [12]). 9Cr1MoVNb and 12Cr1MoVW steels were subjected to two normalizing treatments (1100 °C/1 h, 1040 °C/1 h), which lead to different grain sizes, 16 and 22 μm for 9Cr1MoVNb and 32 and 153 μm for 12Cr1MoVW. They were then tempered at 760 °C/1 h or 780 °C/1 h. The specimens were irradiated at 365 °C to 4.5 dpa and 19.5 dpa. The grain sizes, neutron fluence (dpa) and measured DBTT shifts are listed in Table 2.

$\Delta\sigma_y$ and ΔT_y are calculated from the Eqs. (6) and (8). The α, μ, b in Eq. (10) are 0.23, 8.54×10^4 MPa, 0.268 nm [15]. For 9Cr1MoVNb steels, the density of irradiation-induced dislocation loops, voids, precipitates (chi-phase, $Fe_{36}Cr_{12}Mo_{10}$) and their mean

Table 2
Comparison of calculated and measured DBTT shifts in irradiated 9Cr1MoVNb steels with different grain sizes

Materials	Irradiation temperature, °C	Grain size, μm	Fluence, dpa	Exp. ΔDBTT, °C	Cal. ΔDBTT, °C		
					ΔT_y	ΔT_F	Total
9Cr1MoVNb	365	16	0	0/0	0	0	0
			4.5	45/43	11.2	41.8	53
			19.5	45/58	23.4	42.8	66.2
		22	0	0/0	0	0	0
			4.5	53/55	11.2	69.8	81.0
			19.5	76/72	23.4	70.4	93.8
	420	16	35	39/45	31	0.4/13.6*	31.4/44.6
12Cr1MoVW	365	32	0	0/0	0	0	0
			4.5	129/130	96	22	118
			19.5	115/135	158	23	181
		153	0	0/0	0	0	0
			4.5	134/158	96	22	118
			19.5	149/160	158	23	181
	420	32	35	87/107	191	0.8/16*	191.8/207

sizes are $5\times10^{19}/m^3$, $6\times10^{20}/m^3$, $8.6\times10^{20}/m^3$, 100 nm, 30 nm, 10 nm, respectively [12]. For the 12Cr1MoVW steels, the density of irradiation-induced dislocation loops, voids, precipitates (α' phase and chi-phase) and their mean sizes are $5\times10^{20}/m^3$, $5\times10^{18}/m^3$, $1.5\times10^{22}/m^3$ (α' phase), $6.1\times10^{20}/m^3$ (chi-phase), 100 nm, 30 nm, 5 nm, 13 nm, respectively [12]. There are some $M_{23}C_6$ and MC carbides existing in both steels, but the irradiation does not result in any obvious change of their densities or mean sizes. Thus, their contribution to $\Delta\sigma_y$ is not considered. It should be pointed out that the data used here were obtained from the specimens irradiated at 420 °C to 35 dpa. The irradiation-induced microstructures are similar at the two temperatures, but at 365 °C, the mean sizes of loops, voids and precipitates are smaller, and the densities are higher [13], but this is not quantified In view of the absence of hard data, it is assumed that the defect densities are the same of 365 and 420 °C. According to the case in ferritic pressure vessel steels (VVER) [14], $\Delta\sigma_y = AF^{1/3}$, where F is neutron fluence. The experimental data are fitted and the corresponding yield stress increases at 4.5 and 19.5 dpa for the 9Cr and 12Cr steels, respectively, can be deduced. Comparing the calculated ΔT_y and measured DBTT shifts, it is found that the calculated ΔT_y is almost equivalent to the DBTT shift value for 12Cr steels, but is only half or less for 9Cr steels. This implies that there is an additional contribution to the hardening contribution in 9Cr steels. The concentration of Ni in 9Cr1MoVNb is very low (~0.09%), and thus the number of He atoms produced from transmutation reactions is negligible. The strong hardening contribution in 12Cr1MoVW steels comes mainly from the irradiation-induced high density of α' phase.

The irradiation-induced P segregation is calculated from Eqs. (1)–(3). Free C concentrations used for 9Cr1MoVNb and 12Cr1MoVW steels are 10 and 20 appm, which are estimated using MTData thermodynamic software package [17]. The method for the determination of free C concentration is taken from [3]. For 9Cr1MoVNb, radiation-induced impurity segregation increases with the increase of grain size. Thus ΔT_F increases, see column 5 in Table 2. The calculated radiation-induced P segregation and ΔT_F does not increase with the increase of grain size from 32 to 153 μm (column 5 in Table 2). This is because the high free C concentration in 12Cr1MoVW steels suppresses the P segregation. The calculated DBTT shifts ($\Delta T_y + \Delta T_F$) show good agreement with experiment in the case of 9Cr1MoVNb steels with the grain size of 16 μm, but overestimate slightly for the steels with the grain size of 22 μm. For the 12Cr1Mo steel with the grain size of 32 μm, the predicted result shows good agreement with experimental data at 4.5 dpa but overestimates at 19.5 dpa. For the 12Cr1Mo steel with the grain size of 153 μm, the predicted result underestimates at 4.5 dpa and exhibits a good agreement with experimental data at 19.5 dpa. The predicted DBTT shifts for 9Cr1MoVNb and 12Cr1MoVW steels irradiated up to 100 dpa are shown in Fig. 3. The 9Cr1MoVNb steels show better resistance to irradiation-induced DBTT shift than the 12Cr1MoVW steels. In 420 °C irradiations are relevant because they contribute the material from which the defect density data were produced. Thermal segregation of P becomes important at this temperature and corresponding higher values of P segregation are predicted. However, these irradiations were performed to higher dose (35 dpa) and so segregation would be expected to be higher.

Impurity segregation and its contribution to DBTT shifts is a complicated problem, which can be affected by many factors. Apart from P, other impurity elements, like Si, As and Sn, can segregate to grain boundaries, reducing grain boundary cohesion. In this study, only P is considered. With the increase of neutron irradiation fluence, intergranular segregation of impurity elements increases. Irradiation-induced segregation becomes significant at high neutron fluence. The free C concentration plays an important role in RIS, and can be influenced by material composition, heat treatment

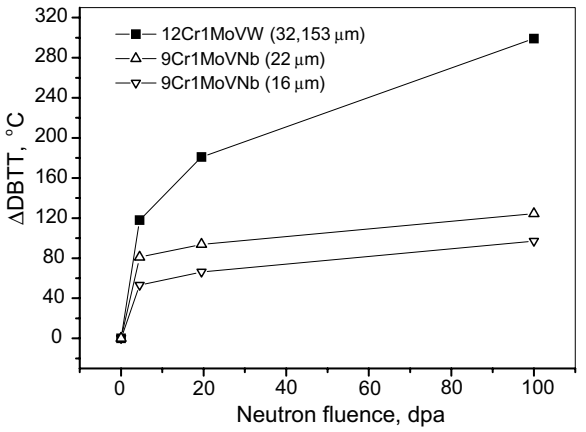

Fig. 3. The predicted DBTT shifts for 9Cr1MoVNb (grain sizes: 16 μm and 22 μm) and 12Cr1MoVW steels (grain sizes: 32 and 153 μm) irradiated up to 100 dpa at 365 °C.

history (e.g., temper, post-welding) and irradiation conditions (e.g., temperature and dose rate).

It is clear that impurity inter-granular segregation on ferritic steels is not the only contributing factor to the DBTT shift. Indeed, in the steels described in experiment, the lower shelf fracture is cleavage and so grain boundary are not important. Also many new fusion first wall alloys like Eurofer, F82H and MANET have very low P level ($<0.005\%$), so inter-granular damage should be insignificant. However, there are indications that in some grades of Eurofer 97 and Eurofer 97 ODS, there are considerable proportions of inter-granular fracture at the lower shelf.

4. Conclusion

A model is presented in this study to predict neutron irradiation-induced impurity segregation at grain boundary and its contribution on the irradiation-induced DBTT shift. The hardening contribution is also considered. The model is applied to forecast the DBTT shifts in irradiated 9Cr1MoVNb and 12Cr1MoVW steels with different grain sizes. Free carbon plays an important role in RIS. The predicted results show good agreement with the experimental data.

Acknowledgement

This work is sponsored by the Loughborough EPSRC-CTA Project (GR/T11296/01).

References

[1] R.L. Klueh, D.R. Harries, High chromium ferritic and martensitic steels for nuclear application, ASTM MONO3, West Conshohocken, PA, 2001.
[2] C.A. English, S.R. Ortner, G. Gage, W.L. Server, S.T. Rosinski, ASTM-STP 1405 (2001) 151.
[3] R.G. Faulkner, R.B. Jones, Z. Lu, P.E.J. Flewitt, Philos. Mag. 85 (2005) 2065.
[4] Z. Lu, R.G. Faulkner, N. Sakaguchi, H. Kinoshita, H. Takahashi, P.E.J. Flewitt, J. Nucl. Mater. 329–333 (2004) 1017.
[5] R.E. Clausing, L. Heatherly, R.G. Faulkner, A.F. Rowcliffe, K. Farrell, J. Nucl. Mater. 141–143 (1986) 978.
[6] R.G. Faulkner, E.A. Little, T.S. Morgan, J. Nucl. Mater. 191–194 (1992) 858.
[7] Z. Lu, R.G. Faulkner, P.E.J. Flewitt, Mater. Sci. Eng. A 437 (2006) 306.
[8] L.S. Shvindlerman, R.G. Faulkner, Interf. Sci. 6 (1998) 213.
[9] C.J. McMahon, V. Vitek, Acta Metall. 27 (1979) 507.
[10] I.V. Gorynin, E.V. Nesterova, V.A. Nikolaev, V.V. Rybin, ASTM STP 1270 (1996) 248.
[11] R.L. Klueh, D.J. Alexander, J. Nucl. Mater. 258–263 (1998) 1269.
[12] J.J. Kai, R.L. Klueh, J. Nucl. Mater. 230 (1996) 116.
[13] R.L. Klueh, J.J. Kai, D.J. Alexander, J. Nucl. Mater. 225 (1995) 175.
[14] Standards of calculation for strength of nuclear power plant equipment and pipelines. PNAE G-7-002-86. M: ENERGO-ATO-MIZDAT, 1989.
[15] R. Kasada, A. Kimura, J. Nucl. Mater. 283–287 (2000) 188.
[16] E. Smith, in: Proceedings Conference on The Physical Basis Field and Fracture, Institute of Physics Society, London, 1966, p. 36.
[17] MTDATA: Metallurgical Thermochemistry Group, National Physical Laboratory, Teddington, London, UK, 1998.